Nonlinear Unmixing of Hyperspectral Images: Models and Algorithms

Nicolas Dobigeon[1], Jean-Yves Tourneret[1], Cédric Richard[2],

José C. M. Bermudez[3], Stephen McLaughlin[4], and Alfred O. Hero[5]

[1] University of Toulouse, IRIT/INP-ENSEEIHT/TéSA, Toulouse, France

`{Nicolas.Dobigeon,Jean-Yves.Tourneret}@enseeiht.fr`

[2] Université de Nice Sophia-Antipolis, OCA, Laboratoire Lagrange, Nice Cedex 2, France

`cedric.richard@unice.fr`

[3] University of Santa Catarina, Florianópolis, SC, Brazil

`j.bermudez@ieee.org`

[4] School of Engineering and Physical Sciences, Heriot-Watt University, Edinburgh, U.K.

`s.mclaughlin@hw.ac.uk`

[5] University of Michigan, Department of EECS, Ann Arbor, USA.

`hero@umich.edu`

Abstract

When considering the problem of unmixing hyperspectral images, most of the literature in the geoscience and image processing areas relies on the widely used linear mixing model (LMM). However, the LMM may be not valid and other nonlinear models need to be considered, for instance, when there are multi-scattering effects or intimate interactions. Consequently, over the last few years, several significant contributions have been proposed to overcome the limitations inherent in the LMM. In this paper, we present an overview of recent advances in nonlinear unmixing modeling.

I. Motivation for nonlinear models

Spectral unmixing (SU) is widely used for analyzing hyperspectral data arising in areas such as: remote sensing, planetary science chemometrics, materials science and other areas of micro-spectroscopy. SU provides a comprehensive and quantitative mapping of the elementary materials that are present in the acquired data. More precisely, SU can identify the spectral signatures of these materials (usually called *endmembers*) and can estimate their relative contributions (or *abundances*) to the measured spectra. Similar to other blind source separation tasks, the SU problem is naturally ill-posed and admits a wide range of admissible solutions. As a consequence, SU is a challenging problem that has received considerable attention in the remote sensing, signal and image processing communities [1]. Hyperspectral data analysis can be *supervised*, when the endmembers are known, or *unsupervised*, when they are unknown. Irrespective of the case, most SU approaches require the definition of the mixing model underlying the observations. A mixing model describes in an analytical fashion how the endmembers combine to form the mixed spectrum measured by the sensor. The abundances parametrize the model. Given the mixing model, SU boils down to estimating the inverse of this formation process to infer the quantities of interest, namely the endmembers and/or the abundances, from the collected spectra. Unfortunately, defining the direct observation model that links these meaningful quantities to the measured data is a non-trivial issue, and requires a thorough understanding of complex physical phenomena. A model based on radiative transfer (RT) could accurately describe the light scattering by the materials in the observed scene [2], but would lead to very complex unmixing problems. Fortunately, invoking simplifying assumptions can lead to exploitable mixing models.

When the mixing scale is macroscopic and each photon reaching the sensor has interacted with just one material, the measured spectrum $\mathbf{y}_p \in \mathbb{R}^L$ in the pth pixel can be accurately described by the linear mixing model

$$\mathbf{y}_p = \sum_{r=1}^{R} a_{r,p}\mathbf{m}_r + \mathbf{n}_p \tag{1}$$

where L is the number of spectral bands, R is the number of endmembers present in the image, $\mathbf{m}_r$ is the spectral signatures of the rth endmember, $a_{r,p}$ is the abundance of the rth material in the pth pixel and $\mathbf{n}_p$ is an additive term associated with the measurement noise and the modeling error. The abundances can be interpreted as the relative areas occupied by the materials in a given image pixel [3]. Thus it is natural to consider additional constraints regarding the abundance coefficients $a_{r,p}$

$$\begin{cases} a_{r,p} \geq 0, & \forall p, \ \forall r \\ \sum_{r=1}^{R} a_{r,p} = 1, & \forall p \end{cases} \tag{2}$$

In that case, SU can be formulated as a constrained blind source separation problem, or constrained linear regression, depending on the prior knowledge available regarding the endmember spectra.

Due to the relative simplicity of the model and the straightforward interpretation of the analysis results, LMM-based unmixing strategies predominate in the literature. All of these techniques have been shown to be very useful whenever the LMM represents a good approximation to the actual mixing. There are, however, practical situations in which the LMM is not a suitable approximation [1]. As an illustrative example, consider a real hyperspectral image, composed of $L = 160$ spectral bands from the visible to near infrared, acquired in 2010 by the airborne Hyspex hyperspectral sensor over Villelongue, France. This image, with a spatial resolution of 0.5m, is represented in Fig. 1 (top). From primary inspection and prior knowledge coming from available ground truth, the 50×50 pixel region of interest depicted in Fig. 1 (bottom, right) is known to be composed of mainly $R = 3$ macroscopic components (oak tree, chestnut tree and an additional non-planted-tree component). When considering the LMM to model the interactions between these $R = 3$ components, all the observed pixels should lie in a 2-dimensional linear subspace, that can be easily identified by a standard principal component analysis (PCA). Conversely, if nonlinear effects are present in the considered scene, the observed data may belong to a 2-dimensional nonlinear manifold. In that case, more complex nonlinear dimension reduction procedures need to be considered. The accuracy of these dimension reduction procedures in representing the dataset into a 2-dimensional linear or nonlinear subspace can be evaluated thanks to the average reconstruction error (ARE), defined as

$$\text{ARE} = \sqrt{\frac{1}{LP} \sum_{n=1}^{N} \|\mathbf{y}_n - \hat{\mathbf{y}}_n\|^2} \tag{3}$$

where $\mathbf{y}_n$ are the observed pixels and $\hat{\mathbf{y}}_n$ the corresponding estimates. Here we contrast two approaches, a locally linear Gaussian process latent variable model (LL-GPLVM) introduced in [4] and PCA. When using PCA to represent the data, the obtained ARE is 8.4×10^{-3} while using the LL-GPLVM, the ARE is reduced to 7.9×10^{-3}. This demonstrates that the investigated dataset should be preferably represented in a nonlinear subspace, as clearly demonstrated in Fig. 1 (bottom, left), where the nonlinear simplex identified by the fully constrained LL-GPLVM has been represented as blue lines.

Consequently, more complex mixing models need to be considered to cope with nonlinear interactions. These models are expected to capture important nonlinear effects that are inherent characteristics of hyperspectral images in several applications. They have proven essential to unveil meaningful information for the geoscience community [5]–[10]. Several approximations to the RT theory have been proposed, such as Hapke's bidirectional model [3]. Unfortunately, these models require highly non-linear and integral formulations that hinder practical implementations of unmixing techniques. To overcome these difficulties, several physics-based approximations of Hapke's model have been
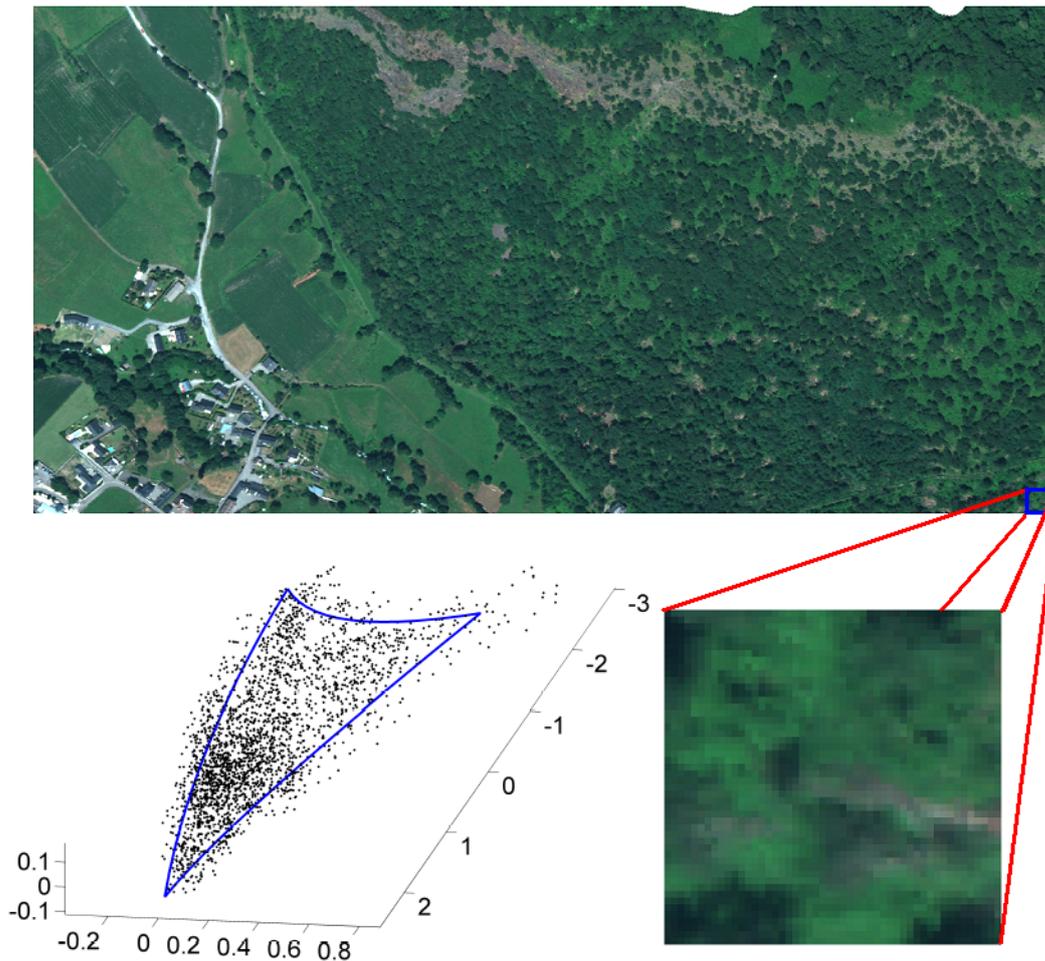
Fig. 1. Top: real hyperspectral Madonna data acquired by the Hyspex hyperspectral scanner over Villelongue, France. Bottom, right: the region of interest shown in true colors. Bottom, left: Representation of the $N = 2500$ pixels (black dots) of the data and boundaries of the estimated nonlinear simplex (blue lines).

proposed, mainly in the spectroscopy literature (e.g., see [3]). However, despite their wide interest, these approximations still remain difficult to apply for automated hyperspectral imaging. In particular, for such models, there is no unsupervised nonlinear unmixing algorithm able to jointly extract the endmembers from the data and estimate their relative proportions in the pixels. Meanwhile, several approximate but exploitable nonlinear mixing models have been recently proposed in the remote sensing and image processing literatures. Some of them are similarly motivated by physical arguments, such as the class of bilinear models introduced later. Others exploit a more flexible non-linear mathematical model to improve unmixing performance. Developing effective unmixing algorithms based on nonlinear mixing models represents a challenge for the signal and image processing community. Supervised and unsupervised algorithms need to be designed to cope with nonlinear transformations that can be partially or totally unknown. Solving the nonlinear unmixing problem requires innovative approaches to existing signal processing techniques.
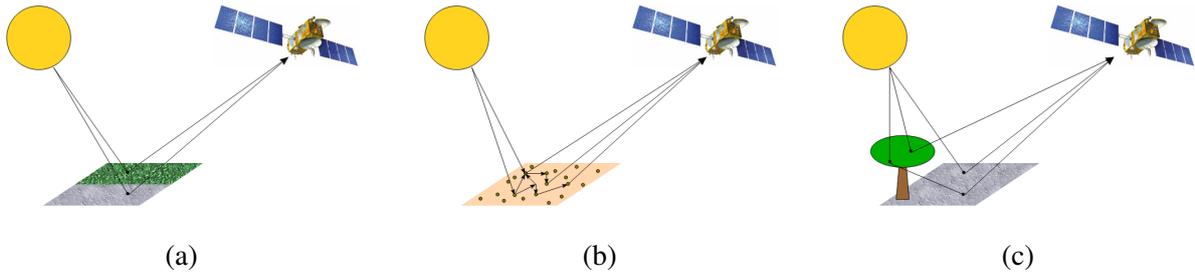
Fig. 2. (a) Linear mixing model: the imaged pixel is composed of two materials. (b) Intimate mixture: the imaged pixel is composed of a microscopic mixture of several constituents. (c) Bilinear model: the imaged pixel is composed of two endmembers, namely tree and soil. In addition to the individual contribution of each material, bilinear interactions between the tree and the soil reach the sensor.

More than 10 years after Keshava and Mustard's comprehensive review article on spectral unmixing [11], this article provides an updated review focusing on non-linear unmixing techniques introduced in the past decade. In [11], the problem on nonlinear mixtures was thoroughly addressed but, at that time, very few algorithmic solutions were available. Capitalizing on almost one decade of advances in solving the linear unmixing problem, scientists from the signal and image processing communities have developed, and continue to do so, automated tools to extract endmembers from nonlinear mixtures, and to quantify their proportions in nonlinearly mixed pixels. The paper is organized as follows. The principal nonlinear mixing models are presented in the next section. Then the most popular nonlinear unmixing algorithms are reviewed. Model-based and model-free algorithms are considered. Existing solutions for supervised and unsupervised unmixing are also discussed. At the end of this paper, we present some recent strategies for detection of nonlinear mixtures in hyperspectral data. Finally, challenges and future directions for hyperspectral unmixing are reported in the conclusions.

II. NON LINEAR MODELS

In [1], it is explained that linear mixtures are reasonable when two assumptions are wholly fulfilled. First the mixing process must occur at a macroscopic scale [12]. Secondly, the photons that reach the sensor must interact with only one material, as is the case in checkerboard type scenes [13]. An illustration of this model is depicted in Fig. 2(a) for a scene composed of two materials. When one of these two assumptions does not hold, different nonlinear effects may occur. Two families of nonlinear models are described in what follows.

A. Intimate mixtures

The first assumption for linear mixtures is a macroscopic mixing scale. However, there are common situations when interactions occur at a microscopic level. The spatial scales involved are typically

smaller than the path length followed by the photons. The materials are said to be intimately mixed [3]. Such mixtures have been observed and studied for some time, e.g., for imaged scenes composed of sand or mineral mixtures [14]. They have been advocated for analyzing mixtures observed in laboratory [15]. Based on RT theory, several theoretical frameworks have been derived to accurately describe the interactions suffered by the light when encountering a surface composed of particles.

An illustration of these interactions is represented in Fig. 2(b). Probably the most popular approaches dealing with intimate mixtures are those of Hapke in [3] since they involve meaningful and interpretable quantities that have physical significance. Based on these concepts, several simplified nonlinear mixing models have been proposed to relate the measurements to some physical characteristics of the endmembers and to their corresponding abundances (that are associated with the relative mass fractions for intimate mixtures). In [2], the author derives an analytical model to express the measured reflectances as a function of parameters intrinsic to the mixtures, e.g., the mass fractions, the characteristics of the individual particles (density, size) and the single-scattering albedo. Other popular approximating models include the discrete-dipole approximation [16] and the Shkuratov's model [17] (interested readers are invited to consult [3] or the more signal processing-oriented papers [18], [19]). However these models also strongly depend on parameters inherent to the experiment since it requires the perfect knowledge of the geometric positioning of the sensor with respect to the observed sample. This dependency upon external parameters makes the inversion (i.e., the estimation of the mass fractions from the collected spectra) very difficult to implement and, obviously, even more challenging in a unsupervised scenario, i.e., when the spectral signatures of the materials are unknown and need to be also recovered.

More generally, it is worth noting that the first requirement of having a macroscopic mixing scale is intrinsically related to the definition of the endmembers. Indeed, defining a pure material requires specification of the spatial or spectral resolution, which is application dependent. Consider, for example, a simple scene composed of 3 materials A, B and C. It is natural to expect retrieval of these components individually when analyzing the scene. However, in other circumstances, one may be interested in the material components themselves, for instance, A_1, A_2, B_1, B_2, C_1 and C_2 if we assume that each material is composed of 2 constituents. In that case, pairs of subcomponents combine and, by performing unmixing, one might also be interested in recovering each of these 6 components. Conversely, it may be well known that the material A can never be present in the observed scene without the material B. In such case, unmixing would consist of identifying the couple $A + B$ and C, without distinguishing the subcomponent A from the subcomponent B. This issue is frequently encountered in automated spectral unmixing. In each scenario, it is clear that when more details are desired, the mixtures should not occur at a macroscopic scale. To circumvent this difficulty in defining the mixture scale, it makes sense to associate pure components with individual instances

whose resolutions have the same order of magnitude than the sensor resolution. For example, a patch of sand of spatially homogeneous composition can be considered as a unique pure component. In that case, most of the interactions occurring in most of the scenes of interest can be reasonably assumed to occur at a macroscopic level, at least when analyzing airborne and spaceborne remotely sensed images.

B. Bilinear models

Another type of nonlinear interaction occurs at a macroscopic scale, in particular in so-called *multilayered* configurations. One may encounter this nonlinear model when the light scattered by a given material reflects off other materials before reaching the sensor. This is often the case for scenes acquired over forested areas, where there may be many interactions between the ground and the canopy. An archetypal example of this kind of scene is shown in Fig. 2(c).

Several models have been proposed to analytically describe these interactions. They consist of including powers of products of reflectance. However they are usually employed such that interactions of orders greater than two are neglected. The resulting models are known as the family of the bilinear mixing models. Mathematically, for most of these bilinear models, the observed spectrum $\mathbf{y}_p \in \mathbb{R}^L$ in L spectral bands for the ith pixel is approximated by the following expansion

$$\mathbf{y}_p = \sum_{r=1}^{R} a_{r,p} \mathbf{m}_r + \sum_{i=1}^{R-1} \sum_{j=i+1}^{R} \beta_{i,j,p} \mathbf{m}_i \odot \mathbf{m}_j + \mathbf{n}_p. \tag{4}$$

where $\odot$ stands for the termwise (Hadamard) product

$$\mathbf{m}_i \odot \mathbf{m}_j = \begin{pmatrix} m_{1,i} \\ \dots \\ m_{L,i} \end{pmatrix} \odot \begin{pmatrix} m_{1,j} \\ \dots \\ m_{L,j} \end{pmatrix} = \begin{pmatrix} m_{1,i} m_{1,j} \\ \dots \\ m_{L,i} m_{L,j} \end{pmatrix}$$

In the right-hand side of (4), the first term, also found in (1), summarizes the linear contribution in the mixture while the second term models nonlinear interactions between the materials. The coefficient $\beta_{i,j,p}$ adjusts the amount of nonlinearities between the components $\mathbf{m}_i$ and $\mathbf{m}_j$ in the pth pixel. Several alternatives for imposing constraints on these nonlinear coefficients have been suggested. Similarly to [10], Nascimento and Dias assume in [20] that the (linear) abundance and nonlinearity coefficients obey

$$\begin{cases} a_{r,p} \geq 0, & \forall p, \ \forall r \\ \beta_{i,j,p} \geq 0, & \forall p, \ \forall i \neq j \\ \sum_{r=1}^{R} a_{r,p} + \sum_{i=1}^{R-1} \sum_{j=i+1}^{R} \beta_{i,j,p} = 1. \end{cases} \tag{5}$$

It is worth noting that, from (5), this Nascimento model (NM), also used in [21], can be interpreted as a linear mixing model with additional virtual endmembers. Indeed, considering $\mathbf{m}_i \odot \mathbf{m}_j$ as a pure

component spectral signature with corresponding abundance $\beta_{i,j,p}$, the model in (5) can be rewritten

$$\mathbf{y}_p = \sum_{s=1}^{\tilde{R}} \tilde{a}_{s,p} \tilde{\mathbf{m}}_s + \mathbf{n}_p$$

with the positivity and additivity constraints in (2) where

$$\begin{cases} \tilde{a}_{s,p} \triangleq a_{r,p}, & \tilde{\mathbf{m}}_s \triangleq \mathbf{m}_r & s = 1, \ldots, R \\ \tilde{a}_{s,p} \triangleq \beta_{i,j,p}, & \tilde{\mathbf{m}}_s \triangleq \mathbf{m}_i \odot \mathbf{m}_j & s = R+1, \ldots, \tilde{R} \end{cases}$$

and $\tilde{R} = \frac{1}{2}R(R+1)$. This NM reduces to the LMM when $\tilde{a}_{s,p} = 0$ for $s = R+1, \ldots, \tilde{R}$.

Conversely, in [9], Fan and his co-authors have fixed the nonlinearity coefficients as functions of the (linear) abundance coefficients themselves: $\beta_{i,j,p} = a_{i,p}a_{j,p}$ ($i \neq j$). The resulting model, called the Fan Model (FM) in what follows, is thus fully described by the mixing equation

$$\mathbf{y}_p = \sum_{r=1}^{R} a_{r,p}\mathbf{m}_r + \sum_{i=1}^{R-1} \sum_{j=i+1}^{R} a_{i,p}a_{j,p}\mathbf{m}_i \odot \mathbf{m}_j + \mathbf{n}_p \tag{6}$$

subject to the constraints in (2). One argument to explain the direct relation between the abundances and the nonlinearity coefficients is the following: if the ith endmember is absent in the pth pixel, then $a_{i,p} = 0$ and there are no interactions between $\mathbf{m}_i$ and the other materials $\mathbf{m}_j$ ($j \neq i$). More generally, it is quite natural to assume that the quantity of nonlinear interactions in a given pixel between two materials is directly related to the quantity of each material present in that pixel. However, it is clear that this model does not generalize the LMM, which can be a restrictive property.

More recently, to alleviate this issue, the generalized bilinear model (GBM) has been proposed in [22] by setting $\beta_{i,j,p} = \gamma_{i,j,p}a_{i,p}a_{j,p}$

$$\mathbf{y}_p = \sum_{r=1}^{R} a_{r,p}\mathbf{m}_r + \sum_{i=1}^{R-1} \sum_{j=i+1}^{R} \gamma_{i,j,p}a_{i,p}a_{j,p}\mathbf{m}_i \odot \mathbf{m}_j + \mathbf{n}_p. \tag{7}$$

where the interaction coefficient $\gamma_{i,j,p} \in (0,1)$ quantifies the nonlinear interaction between the spectral components $\mathbf{m}_i$ and $\mathbf{m}_j$. This model has the same interesting characteristic as the FM: the amount of nonlinear interactions is governed by the presence of the endmembers that linearly interact. In particular, if an endmember is absent in a pixel, there is no nonlinear interaction supporting this endmember. However, it also has the significant advantage of generalizing both the LMM when $\gamma_{i,j,p} = 0$ and the FM when $\gamma_{i,j,p} = 1$. Having $\gamma_{i,j,p} > 0$ indicate that only constructive interactions are considered.

For illustration, synthetic mixtures of $R = 3$ spectral components have been randomly generated according to the LMM, NM, FM and GBM. The resulting data set are represented in the space spanned by the three principal eigenvectors (associated with the three largest eigenvalues of the sample covariance matrix of the data) identified by a principal component analysis in Fig. 3. These plots illustrate an interesting property for the considered dataset: the spectral signatures of the pure

components are still extremal points, i.e., vertices of the clusters, in the cases of FM and GBM mixtures contrary to the NM. In other words, geometrical endmember extraction algorithms (EEAs) and, in particular, those that are looking for the simplex of largest volume (see [23] for details), may still be valid for the FM and the GBM under the assumption of weak nonlinear interactions.

All these bilinear models only include between-component interactions $\mathbf{m}_i \odot \mathbf{m}_j$ with $i \neq j$ but no within-component interactions $\mathbf{m}_i \odot \mathbf{m}_i$. Finally, in [24], the authors derived a nonlinear mixing model using a RT model applied to a simple canyon-like urban scene. Successive approximations and simplifying assumptions lead to the following linear-quadratic mixing model (LQM)

$$\mathbf{y}_p = \sum_{r=1}^{R} a_{r,p}\mathbf{m}_r + \sum_{i=1}^{R}\sum_{j=i}^{R} \beta_{i,j,p}\mathbf{m}_i \odot \mathbf{m}_j + \mathbf{n}_p \tag{8}$$

with the positivity and additivity constraints in (2) and $\beta_{i,j,p} \in (0,1)$. This model is similar to the general formulation of the bilinear models in (4), with the noticeable difference that the nonlinear contribution includes quadratic terms $\mathbf{m}_i \odot \mathbf{m}_i$. This contribution also shows that it is quite legitimate to include the termwise products $\mathbf{m}_i \odot \mathbf{m}_j$ as additional components of the standard linear contribution, which is the core of the bilinear models described in this section.

C. Other approximating physics-based models

To describe both macroscopic and microscopic mixtures, [25] introduces a dual model composed of two terms

$$\mathbf{y}_p = \sum_{r=1}^{R} a_{r,p}\mathbf{m}_r + a_{R+1,p}\mathcal{R}\left(\sum_{r=1}^{R} f_{r,p}\mathbf{w}_r\right) + \mathbf{n}_p.$$

The first term is similar to the one encountered in LMM and comes from the macroscopic mixing process. The second one, considered as an additional endmember with abundance $a_{R+1,p}$, describes the intimate mixture by the average single-scattering albedo [2] expressed in the reflective domain by the mapping $\mathcal{R}(\cdot)$.

On the use of geometrical LMM-based EEAs to identify nonlinearly mixed endmembers

The first automated spectral unmixing algorithms, proposed in the 1990's, were based on geometrical concepts and were designed to identify endmembers as pure pixels (see [1] and [23] for comprehensive reviews of geometrical linear unmixing methods). It is worth noting that this class of algorithms does not explicitly rely on the assumption of pixels coming from linear mixtures. They only search for endmembers as extremal points in the hyperspectral dataset. Provided there are pure pixels in the analyzed image, this might indicate that some of these geometrical approaches can be still valid for nonlinear mixtures that preserve this property, such as the GBM and the FM as illustrated in Fig. 3.
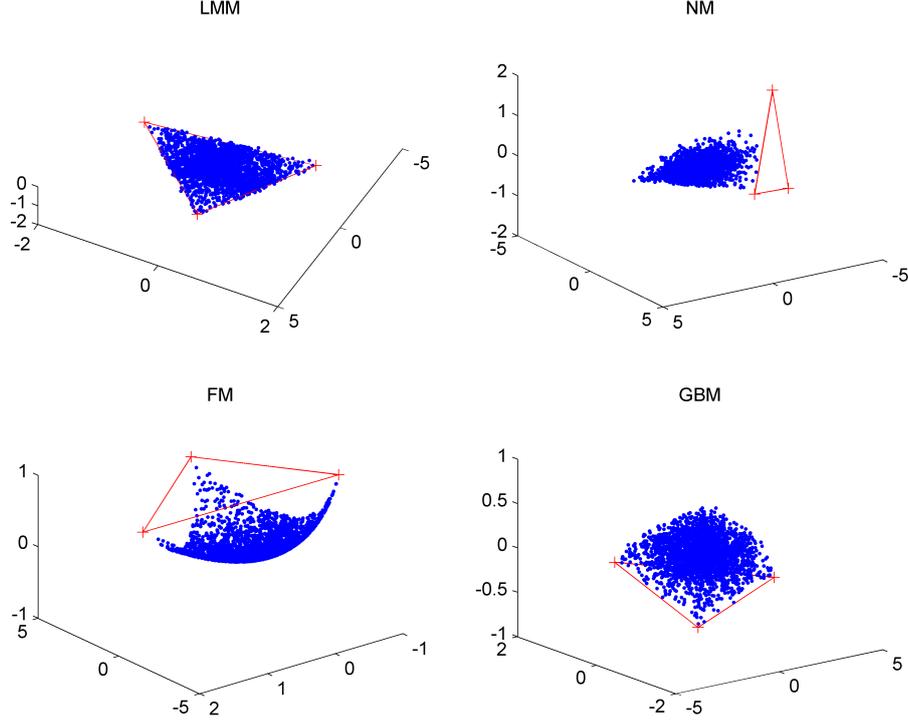
Fig. 3. Clusters of observations generated according to the LMM, the NM, the FM and the GBM (blue) and the corresponding endmembers (red crosses).

Altmann *et al.* have proposed in [26] an approximating model able to describe a wide class of nonlinearities. This model is obtained by performing a second-order expansion of the nonlinearity defining the mixture. More precisely, the pth observed pixel spectrum is defined as a nonlinear transformation $\mathbf{g}_p(\cdot)$ of a linear mixture of the endmember spectra

$$\mathbf{y}_p = \mathbf{g}_p\left(\sum_{r=1}^{R} a_{r,p}\mathbf{m}_r\right) + \mathbf{n}_p \tag{9}$$

where the nonlinear function $\mathbf{g}_p$ is defined as a second order polynomial nonlinearity parameterized by the unique nonlinearity parameter b_p

$$\begin{aligned} \mathbf{g}_p: \quad & (0,1)^L \quad \to \mathbb{R}^L \\ & \mathbf{x} \quad \mapsto \left[x_1 + b_p x_1^2, \ldots, x_L + b_p x_L^2\right]^T \end{aligned} \tag{10}$$

This model can be rewritten

$$\mathbf{y}_p = \mathbf{M}\mathbf{a}_p + b_p\left(\mathbf{M}\mathbf{a}_p\right) \odot \left(\mathbf{M}\mathbf{a}_p\right) + \mathbf{n}_p$$

where $\mathbf{M} = [\mathbf{m}_1, \ldots, \mathbf{m}_R]$ and $\mathbf{a}_p = [a_{1,p}, \ldots, a_{R,p}]^T$. The parameter b_p tunes the amount of nonlinearity present in the pth pixel of the image and this model reduces to the standard LMM when $b_p = 0$. It can be easily shown that this polynomial post-nonlinear model (PPNM) includes

bilinear terms $\mathbf{m}_i \odot \mathbf{m}_j$ ($i \neq j$) similar to those defining the FM, NM and GBM, as well as quadratic terms $\mathbf{m}_i \odot \mathbf{m}_i$ similar to the LQM in (8). This PPNM has been shown to be sufficiently flexible to describe most of the bilinear models introduced in this section [26].

D. Limitations a pixel-wise nonlinear SU

Having reviewed the above physics-based models, an important remark must be made. It is important to note that these models do not take into account spatial interactions from materials present in the neighborhood of the targeted pixel. It means that these bilinear models only consider scattering effects in a given pixel induced by components that are present in this specific pixel. This is a strong simplifying assumption that allows the model parameters (abundance and nonlinear coefficients) to be estimated pixel-by-pixel in the inversion step. Note however that the problem of taking adjacency effects into account, i.e., nonlinear interactions coming from spectral interference caused by atmospheric scattering, has been addressed in an unmixing context in [27].

III. NONLINEAR UNMIXING ALGORITHMS

Significant promising approaches have been proposed to nonlinearly unmix hyperspectral data. A wide class of nonlinear unmixing algorithms rely explicitly on a nonlinear physics-based parametric model, as detailed earlier. Others do not require definition of the mixing model and rely on very mild assumptions regarding the nonlinearities. For these two classes of approaches, unmixing algorithms have been considered under two different scenarios, namely supervised or unsupervised, depending on the available prior knowledge on the endmembers. When the endmembers are known, supervised algorithms reduce to estimating the abundance coefficients in a single supervised inversion step. In this case, the pure spectral signatures present in the scene must have been previously identified. For instance, they use prior information or suboptimal linear EEA. Indeed, as previously noted, when considering weakly nonlinearly mixed data, the LMM-based EEA may produce good endmember estimates when there are pure pixels in the dataset. In contrast, an unsupervised unmixing algorithm jointly estimates the endmembers and the abundances. Thus the unmixing problem becomes even more challenging, since a blind source separation problem must be solved.

A. Model-based parametric nonlinear unmixing algorithms

Given a nonlinear parametric model, SU can be formulated as a constrained nonlinear regression or a nonlinear source separation problem, depending on whether the endmember spectral signatures are known or not. When dealing with intimate mixtures, some authors have proposed converting the measured reflectance into a single scattering albedo average; since this obeys a linear mixture, the mass fractions associated with each endmember can be estimated using a standard linear unmixing

algorithm. This is the approach adopted in [15] and [18] for known and unknown endmembers, respectively. To avoid the functional inversion of the reflectance measurements into the single scattering albedo, a common approach is to use neural-networks (NN) to learn this nonlinear function. This is the strategy followed by Guilfoyle *et al.* in [28], for which several improvements have been proposed in [29] to reduce the computationally intensive learning step. In these NN-based approaches, the endmembers are assumed to be known a-priori, and are required to train the NN. Other NN-based algorithms have been studied in [30]–[33].

For the bilinear models introduced previously, supervised nonlinear optimization methods have been developed based on the assumption that the endmember matrix $\mathbf{M}$ is known. When the observed pixel spectrum $\mathbf{y}_p$ is related to the parameters of interest $\boldsymbol{\theta}_p$ (a vector containing the abundance coefficients as well as any other nonlinearity parameters) through the function $\boldsymbol{\varphi}(\mathbf{M}, \cdot)$, unmixing the pixel $\mathbf{y}_p$ consists of solving the following minimization problem

$$\hat{\boldsymbol{\theta}}_p = \underset{\boldsymbol{\theta}}{\operatorname{argmin}} \left\| \mathbf{y}_p - \boldsymbol{\varphi}(\mathbf{M}, \boldsymbol{\theta}) \right\|_2^2. \tag{11}$$

This problem raises two major issues: i) the nonlinearity of the criterion resulting from the underlying nonlinear model $\boldsymbol{\varphi}(\cdot)$ and ii) the constraints that have to be satisfied by the parameter vector $\boldsymbol{\theta}$. Since the NM can be interpreted as a linear mixing model with additional virtual endmembers, estimation of the parameters can be conducted with a linear optimization method as in [20]. In [9], [34] dedicated to FM and GBM, the authors propose to linearize the objective criterion via a first-order Taylor series expansion of $\boldsymbol{\varphi}(\cdot)$. Then, the fully constrained least square (FCLS) algorithm of [35] can be used to estimate parameter vector $\boldsymbol{\theta}$. An alternative algorithmic scheme proposed in [34] consists of resorting to a gradient descent method where the step-size parameter is adjusted by a constrained line search procedure enforcing the constraints inherent to the mixing model. Another strategy initially introduced in [22] for the GBM is based on Monte Carlo approximations, developed in a fully Bayesian statistical framework. The Bayesian setting has the great advantage of providing a convenient way to include the parameter constraints within the estimation problem, by defining appropriate priors for the parameters. This strategy has been also considered to unmix the PPNM [26].

When the spectral signatures $\mathbf{M}$ involved in these bilinear models need also to be identified in addition to the abundances and nonlinearity parameters, more ambitious unmixing algorithms need to be designed. In [36], the authors differentiate the NM to implement updating rules that generalize the SPICE algorithm introduced in [37] for the linear mixing model. Conversely, NMF-based iterative algorithms have been advocated in [38] for the GBM defined in (7), and in [24] for the LQM described in (8). More recently, an unsupervised version of the Bayesian PPNM-based unmixing algorithm initially introduced in [26] has been investigated in [39].

Adopting a geometrical point-of-view, Heylen and Scheunders propose in [40] an integral formula-

tion to compute geodesic distances on the nonlinear manifold induced by the GBM. The underlying idea is to derive an EEA that identifies the simplex of maximum volume contained in the manifold defined by the GBM-mixed pixels.

B. Model-free nonlinear unmixing algorithms

When the nonlinearity defining the mixing is unknown, the SU problem becomes even more challenging. In such cases, when the endmember matrix $\mathbf{M}$ is fixed a priori, a classification approach can be adopted to estimate the abundance coefficients which can be solved using support vector machines [41], [42]. Conversely, when the endmember signatures are not known, a geometrical-based unmixing technique can be used, based on graph-based approximate geodesic distances [43], or manifold learning techniques [44], [45]. Another promising approach is to use nonparametric methods based on reproducing kernels [46]–[51] or on Gaussian processes [4] to approximate the unknown nonlinearity. These two later techniques are described below.

Nonlinear algorithms operating in reproducing kernel Hilbert spaces (RKHS) have received considerable interest in the machine learning community, and have proved their efficiency in solving nonlinear problems. Kernel-based methods have been widely considered for detection and classification in hyperspectral images. Surprisingly, nonlinear unmixing approaches operating in RKHS have been investigated in a less in-depth way. The algorithms derived in [46], [47] were mainly obtained by replacing each inner product between endmember spectra in the cost functions to be optimized by a kernel function. This can be viewed as a nonlinear distortion map applied to the spectral signature of each material, independently of their interactions. This principle can be extremely efficient in solving detection and classification problems as a proper distortion can increase the detectability or separability of some patterns. It is however of little physical interest in solving the unmixing problem because the nonlinear nature of the mixtures is not only governed by individual spectral distortions, but also by nonlinear interactions between the materials. In [48], a new kernel-based paradigm was proposed to take the nonlinear interactions of the endmembers into account, when these endmembers are assumed to be a priori known. It solves the optimization problem

$$\min_{\psi_{\boldsymbol{\theta}} \in \mathcal{H}} \sum_{\ell=1}^{L} \left[y_{\ell,p} - \psi_{\boldsymbol{\theta}}(\mathbf{m}_{\lambda_\ell}) \right]^2 + \mu \|\psi_{\boldsymbol{\theta}}\|_{\mathcal{H}}^2 \tag{12}$$

where $\mathbf{m}_{\lambda_\ell}$ is the vector of the endmember signatures at the ℓ-th frequency band, namely, $\mathbf{m}_{\lambda_\ell} = [m_{\ell,1}, \ldots, m_{\ell,R}]^T$, with $\mathcal{H}$ a given functional space, and μ a positive parameter that controls the trade-off between regularity of the function $\psi_{\boldsymbol{\theta}}(\cdot)$ and fitting. Again, $\boldsymbol{\theta}$ is a vector containing the abundance coefficients as well as any other nonlinearity parameters. It is interesting to note that (12) is the functional counterpart to (11), where $\psi_{\boldsymbol{\theta}}(\cdot)$ defines the nonlinear interactions between the

endmembers assumed to be known in [48]. Clearly, this strategy may fail if the functional space $\mathcal{H}$ is not chosen appropriately. A successful strategy is to define $\mathcal{H}$ as an RKHS in order to exploit the so-called kernel trick. Let $\kappa(\cdot, \cdot)$ be the reproducing kernel of $\mathcal{H}$. The RKHS $\mathcal{H}$ must be carefully selected via its kernel in order to make it flexible enough to capture wide classes of nonlinear relationships, and to reliably interpret a variety of experimental measurements. In order to extract the mixing ratios of the endmembers, the authors in [48] focus their attention on partially linear models, resulting in the so-called K-HYPE SU algorithm. More precisely, the function $\psi_{\boldsymbol{\theta}}(\cdot)$ in problem (12) is defined by an LMM parameterized by the abundance vector $\mathbf{a}$, combined with a nonparametric term,

$$\psi_{\boldsymbol{\theta}}(\mathbf{m}_{\lambda_\ell}) = \mathbf{a}^\top \mathbf{m}_{\lambda_\ell} + \psi_{\mathrm{nlin}}(\mathbf{m}_{\lambda_\ell}) \tag{13}$$

possibly subject to the constraints in (2), where ψ_{nlin} can be any real-valued function of an RKHS denoted by $\mathcal{H}_{\mathrm{nlin}}$. This model generalizes the standard LMM, and mimics the PPNM when $\mathcal{H}_{\mathrm{nlin}}$ is defined to be the space of polynomial functions of degree 2. Remember that the latter is induced by the polynomial kernel $\kappa(\mathbf{m}_{\lambda_\ell}, \mathbf{m}_{\lambda_{\ell'}}) = (\mathbf{m}_{\lambda_\ell}^\top \mathbf{m}_{\lambda_{\ell'}})^q$ of degree $q = 2$. More complex interaction mechanisms can be considered by simply changing $\kappa(\mathbf{m}_{\lambda_\ell}, \mathbf{m}_{\lambda_{\ell'}})$. By virtue of the reproducing kernel machinery, the problem can still be solved in the framework of (12).

Another strategy introduced in [4] considers a kernel-based approach for unsupervised nonlinear SU based on a nonlinear dimensionality reduction using a Gaussian process latent variable model (GPLVM). In this work, the authors have used a particular form of kernel which extends the generalized bilinear model in (7). The algorithm proposed in [4] is unsupervised in the sense that the endmembers contained in the image and the mixing model are not known. Only the number of endmembers is assumed to be known. As a consequence, the parameters to be estimated are the kernel parameters, the endmember spectra and the abundances for all image pixels. The main advantage of GPLVMs is their capacity to accurately model many different nonlinearities. GPLVMs construct a smooth mapping from the space of fractional abundances to the space of observed mixed pixels that preserves dissimilarities. This strategy has been also considered in [51] by Nguyen *et al.*, who solve the so-called pre-image problem [52] studied in the machine learning community. In the SU context, it means that pixels that are spectrally different have different latent variables and thus different abundance vectors. However, preserving local distances is also interesting: spectrally close pixels are expected to have similar abundance vectors and thus similar latent variables. Several approaches have been proposed to preserve similarities, including back-constraints and locally linear embedding.

For illustration, a small set of experiments has been conducted to evaluate some of the model-based and model-free algorithms introduced above. First, 4 synthetic images of size 50×50 have been generated by mixing $R = 3$ endmember spectra (i.e., green grass, olive green paint and galvanized steel metal) extracted from the spectral libraries provided with the ENVI software [53]. These 4

			Mixing models – with pure pixels				Mixing models – w/o pure pixels			
			LMM	PPNM	GBM	FM	LMM	PPNM	GBM	FM
Model-based algo.	LMM	N-FINDR + FCLS	1.42	14.1	7.71	13.4	3.78	13.2	6.83	9.53
		unsupervised MCMC	0.64	12.4	5.71	8.14	0.66	10.9	4.21	3.92
	PPNM	Geodesic + GBA	1.52	10.3	6.04	12.1	4.18	6.04	4.13	3.74
		unsupervised MCMC	0.39	0.73	1.32	2.14	0.37	0.81	1.38	2.25
	GBM	Geodesic + GBA	2.78	14.3	6.01	13.0	4.18	11.1	5.02	1.45
	FM	Geodesic + GBA	13.4	21.8	9.90	3.40	12.2	18.1	7.17	4.97
Geodesic + K-HYPE			2.43	9.71	5.23	11.3	2.44	5.92	3.18	2.58

TABLE I

ABUNDANCE RNMSEs ($\times 10^{-2}$) FOR VARIOUS LINEAR/NONLINEAR UNMIXING SCENARIOS.

images have been generated according to the standard LMM (1), the GBM (7), the FM (6) and the PPNM (9), respectively. For each image, the abundance coefficient vectors $\mathbf{a}_p \triangleq [a_{1,p}, \ldots, a_{3,p}]$ ($p = 1, \ldots, 2500$) have been randomly and uniformly generated in the admissible set defined by the constraints (2). We have also considered the more challenging scenario defined by the assumption that there is no pure pixel (by imposing $a_{r,p} < 0.9$, $\forall r, \forall p$). The nonlinearity coefficients are uniformly drawn in the set $[0, 1]$ for the GBM. The PPNM-parameters b_p, $p = 1 \ldots, P$ have been generated uniformly in the set $[-0.3, 0.3]$. For both scenario (i.e., with of without pure pixels), all images have been corrupted by an additive independent and identically distributed (i.i.d) Gaussian noise of variance $\sigma^2 = 10^{-4}$, which corresponds to an average signal-to-noise ratio of 20dB (note that the usual SNR for most of the spectro-imagers are not below 30dB). Various unmixing strategies have been implemented to recover the endmember signatures and then estimate the abundance coefficients. For supervised unmixing, the N-FINDR algorithm [54] and its nonlinear geodesic-based counterpart [43] have been used to extract the endmembers from linear and nonlinear mixtures, respectively. Then, dedicated model-based strategies were used to recover the abundance fractions. The fully constrained least square (FCLS) algorithm [35] was used for linear mixtures. Gradient-based algorithms (GBA) were used for nonlinear mixtures. The GBA are detailed in [55], [34] and [9] for the PPNM, GBM and FM, respectively. For comparison with supervised unmixing, and to evaluate the impact of having no pure pixels in these images, joint estimations of endmembers and abundances was implemented using the Markov chain Monte Carlo techniques detailed in [56] and [39] for the LMM and PPNM images, respectively. Finally, the model-free supervised K-HYPE algorithm detailed in [48] was also coupled with the nonlinear EEA in [43]. The performance of these unmixing strategies has been evaluated in term of abundance estimation error measured by

$$\text{RNMSE} = \sqrt{\frac{1}{RP} \sum_{n=1}^{N} \|\mathbf{a}_p - \hat{\mathbf{a}}_p\|^2}$$

where $\mathbf{a}_p$ is the nth actual abundance vector and $\hat{\mathbf{a}}_p$ its corresponding estimate. The results are reported in Table I. These results clearly show that the prior knowledge of the actual mixing model underlying the observations is a clear advantage for abundance estimation. However, in the absence of such knowledge, using an inappropriate model-based algorithm may lead to poor unmixing results. In such cases, as advocated before, PPNM seems to be sufficiently flexible to provide reasonable estimates, whatever the mixing model may be. Otherwise, one may prefer to resort to model-free based strategy such as K-HYPE.

IV. DETECTING NONLINEAR MIXTURES

Consideration of nonlinear effects in hyperspectral images can provide more accurate results in terms of endmember and abundance identification. However, working with nonlinear models generally requires a higher computational complexity than approaches based on the LMM. Thus, unmixing linearly mixed pixels using nonlinear models should be avoided. Consequently, it is of interest to devise techniques to detect nonlinearities in the mixing process before applying any unmixing method. Linearly mixed pixels can then be unmixed using linear unmixing techniques, leaving the application of more involved nonlinear unmixing methods to situations where they are really necessary. This section describes approaches that have been recently proposed to detect nonlinear mixing in hyperspectral images.

A. Detection using a polynomial post-nonlinear model (PPNM)

One interesting approach for nonlinearity detection is to assume a parametric nonlinear mixing model that can model different nonlinearities between the endmembers and the observations. A model that has been successfully applied to this end is the PPNM (9) studied in [26], [55]. PPNM assumes the post-nonlinear mixing described in (9) with the polynomial nonlinearity $\mathbf{g}_p$ defined in (10). Hence, the nonlinearity is characterized by the parameter b_p for each pixel in the scene. This parameter can be estimated in conjunction with the abundance vector $\mathbf{a}_p$ and the noise variance σ^2. Denote as $s^2(\mathbf{a}_p, b_p, \sigma^2)$ the variance of the maximum likelihood estimator $\hat{b}_p$ of b. Using the properties of the maximum likelihood estimator, it makes sense to approximate the distribution of $\hat{b}_p$ by the following Gaussian distribution

$$\hat{b}_p \sim \mathcal{N}\left(b_p, s^2(a_p, b_p, \sigma^2)\right).$$

The nonlinearity detection problem can be formulated as the following binary hypothesis testing problem

$$\begin{cases} \mathcal{H}_0 & : \mathbf{y}_p \text{ is distributed according to the LMM (1)} \\ \mathcal{H}_1 & : \mathbf{y}_p \text{ is distributed according to the PPNM (9)} \end{cases} \tag{14}$$

Hypothesis $\mathcal{H}_0$ is characterized by $b_p = 0$ whereas nonlinear models ($\mathcal{H}_1$) correspond to $b_p \neq 0$. Then, (14) can be rewritten as

$$\begin{cases} \mathcal{H}_0 & : \quad \hat{b}_p \sim \mathcal{N}(0, s_0^2) \\ \mathcal{H}_1 & : \quad \hat{b}_p \sim \mathcal{N}(b_p, s_1^2) \end{cases} \tag{15}$$

where $s_0^2 = s^2(\mathbf{a}_p, 0, \sigma^2)$ and $s_1^2 = s^2(\mathbf{a}_p, b_p, \sigma^2)$ with $b_p \neq 0$. Detection can be performed using the generalized likelihood ratio test. This test accepts $\mathcal{H}_1$ (resp. $\mathcal{H}_0$) if the ratio $T \triangleq \hat{b}_p^2 / s_0^2$ is greater (resp. lower) than a threshold η. As shown in [55], the statistic T is approximately normally distributed under the two hypotheses. Consequently, the threshold η can be explicitly related to the probability of false alarm (PFA) and the probability of detection (PD), i.e., the power of the test. However, this detection strategy assumes the prior knowledge of the variances s_0^2 and s_1^2. In practical applications, Altmann *et al.* show that have proposed to modify the previous test strategy as follows [55]

$$\hat{T} = \frac{\hat{b}_p^2}{\hat{s}_0^2} \mathop{\gtrless}_{\mathcal{H}_0}^{\mathcal{H}_1} \eta^* \tag{16}$$

where $\hat{s}_0^2$ can be calculated as

$$\hat{s}_0^2 = \mathrm{CCRLB}(0; \hat{\mathbf{a}}_p, \hat{\sigma}^2) \tag{17}$$

In (17), CCRLB is the constrained Cramér-Rao lower-bound [57] on estimates of the parameter vector $\boldsymbol{\theta} = [\mathbf{a}_p^T, b_p, \sigma^2]^T$ under $\mathcal{H}_0$, and $(\hat{\mathbf{a}}_p, \hat{\sigma}^2)$ is the MLE of $(\mathbf{a}_p, \sigma^2)$. The performance of the resulting test is illustrated in Fig. 4 which shows the pixels detected as linear (red crosses) and nonlinear (blue dots) when generated according to various mixing models (LMM, FM, GBM and PPNM).

B. Robust model-free detection

The detector discussed in the previous section assumes a specific nonlinear mixing model under the alternative hypothesis. However, there are situations where the actual mixing does not obey any available model. It is also possible that there is insufficient information to opt for any existing nonlinearity model. In these cases, it is interesting to address the problem of determining whether an observed pixel is a linear function of endmembers or results from a generic nonlinear mixing.

One may consider the LMM (1) and the hyperplane $\mathcal{P}$ defined by

$$\mathcal{P} : \left\{ \boldsymbol{z}_p \middle| \boldsymbol{z}_p = \mathbf{M}\mathbf{a}_p, \sum_{r=1}^{R} a_{r,p} = 1 \right\}. \tag{18}$$

In the noise-free case, the hyperplane $\mathcal{P}$ lies in an $(R-1)$-dimensional subspace embedding all observations distributed according to the LMM. On the other hand, consider the general nonlinear mixing model

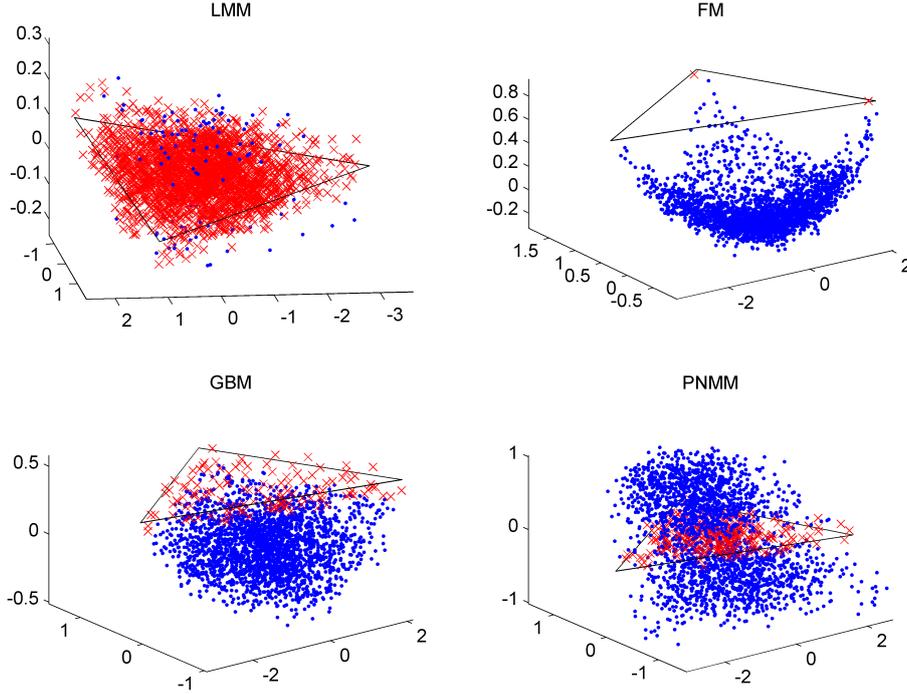$$\mathbf{y}_p = \mathbf{M}\mathbf{a}_p + \boldsymbol{\mu}_p + \mathbf{n}_p \tag{19}$$

Fig. 4. Pixels detected as linear (red crosses) and nonlinear (blue dotted) for the four subimages generated according the LMM, FM, GBM, and PPNM. Black lines depict the simplex corresponding to the noise-free case LMM.

where $\boldsymbol{\mu}_p$ is an $L \times 1$ deterministic vector that does not belong to $\mathcal{P}$, i.e., $\boldsymbol{\mu}_p \notin \mathcal{P}$ and $\mathbf{a}_p$ satisfies the constraints (2). Note that a similar nonlinear mixing model coupled with a group-sparse constraint on $\boldsymbol{\mu}_p$ has been explicitly adopted in [58], [59] to make more robust the unmixing of hyperspectral pixels. In (19), $\boldsymbol{\mu}_p$ can be a nonlinear function of the endmember matrix $\mathbf{M}$ and/or the abundance vector $\mathbf{a}_p$ and should be denoted as $\boldsymbol{\mu}_p(\mathbf{M}, \mathbf{a}_p)$ [60]. However, the arguments $\mathbf{M}$ and $\mathbf{a}_p$ are omitted here for brevity. Given an observation vector $\mathbf{y}_p$, the detection of nonlinear mixtures can be formulated as the following binary hypothesis testing problem

$$\begin{cases} \mathcal{H}_0 & : \quad \mathbf{y}_p \text{ is distributed according to the LMM (1)} \\ \mathcal{H}_1 & : \quad \mathbf{y}_p \text{ is distributed according to the model (19).} \end{cases}$$

Using the statistical properties of the noise $\mathbf{n}_p$, we obtain $\mathrm{E}[\mathbf{y}_p | \mathcal{H}_0] = \mathbf{M}\mathbf{a}_p \in \mathcal{P}$ whereas $\mathrm{E}[\mathbf{y}_p | \mathcal{H}_1] = \mathbf{M}\mathbf{a}_p + \boldsymbol{\mu}_p \notin \mathcal{P}$. As a consequence, it makes sense to consider the squared Euclidean distance

$$\delta^2(\mathbf{y}_p) = \min_{\mathbf{z}_p \in \mathcal{P}} \|\mathbf{y}_p - \mathbf{z}_p\|^2 \tag{20}$$

between the observed pixel $\mathbf{y}_p$ and the hyperplane $\mathcal{P}$ to decide which hypothesis ($\mathcal{H}_0$ or $\mathcal{H}_1$) is true.

As shown in [60], the test statistic $\delta^2(\mathbf{y}_p)$ is distributed according to χ^2 distribution under the two hypotheses $\mathcal{H}_0$ and $\mathcal{H}_1$. The parameters of this distribution depend on the known matrix $\mathbf{M}$, the noise variance σ^2 and the nonlinearity vector $\boldsymbol{\mu}_p$. If σ^2 is known, the distribution of $\delta^2(\mathbf{y}_p)$ is perfectly

known under $\mathcal{H}_0$ and partially known under $\mathcal{H}_1$. In this case, one may employ a statistical test that does not depend on $\boldsymbol{\mu}_p$. This test accepts $\mathcal{H}_1$ (resp. $\mathcal{H}_0$) if the ratio $T \triangleq \delta^2(\mathbf{y}_p)/\sigma^2$ is greater (resp. lower) than a threshold η. As in the PPNM-based detection procedure, the threshold η can be related to the PFA and PD through closed-form expressions. In particular, it is interesting to note that the PD is intrinsically related to a non-Euclidean norm of the residual component $\boldsymbol{\mu}_p$ (see [60, Eq. (11)]), which is unfortunately unknown in most practical applications. If the noise variance σ^2 is unknown, which is the case in most practical applications, one can replace σ^2 with an estimate $\hat{\sigma}^2$, leading to

$$T^* \triangleq \frac{\delta^2(\mathbf{y}_p)}{\hat{\sigma}^2} \underset{\mathcal{H}_0}{\overset{\mathcal{H}_1}{\gtrless}} \eta \tag{21}$$

where η is the threshold computed as previously indicated. The PFA and PD of the test (21) are then explicitly obtained using cumulative distribution functions of the χ^2 distribution. It was shown in [60] that the better the estimation of σ^2, the closer the distributions of T and T^* and thus the closer the performances of the two corresponding tests. Several techniques can be used to estimate σ^2. For instance, $\hat{\sigma}^2$ has been estimated in [60] through an eigen-analysis of the sample covariance matrix of a set of pixels assumed to share the same variance. The value of $\hat{\sigma}^2$ was determined as the average of the smallest eigenvalues of the sample covariance matrix. The accuracy of the estimator is a function of the number of eigenvalues considered. It was shown in [60] that a PFA smaller (resp. larger) than P_{FA}^* is obtained if $\hat{\sigma}^2 > \sigma^2$ (resp. $\hat{\sigma}^2 < \sigma^2$).

V. Conclusions and open challenges

To overcome the intrinsic limitations of the linear mixing model, several recent contributions have been made for modeling of the physical processes that underly hyperspectral observations. Some models attempt to account for between-material interactions affecting photons before they reach the spectro-imager. Based on these models, several parametric algorithms have been proposed to solve the resulting nonlinear unmixing problem. Another class of unmixing algorithms attempts to avoid the use of any rigid nonlinear model by using nonparametric machine learning-inspired techniques. The price to pay for handling nonlinear interactions induced by multiple scattering effects or intimate mixtures is the computational complexity and a possible degradation of unmixing performance when processing large hyperspectral images. To overcome these difficulties, one possible strategy consists of detecting pixels subjected to nonlinear mixtures in a pre-processing step. The pixels detected as linearly mixed can then benefit from the huge and reliable literature dedicated to the linear unmixing problem. The remaining pixels (detected as nonlinear) can then be the subject of particular attention.

This paper has described developments methods in nonlinear mixing for hyperspectral imaging. Several important several interesting challenges remain. First of all, better integration of algorithmic approaches and physical models have the potential to greatly improve non-linear unmixing perfor-

mance. By fully accounting for complex RT effects, such as scattering, dispersion, and beam interaction depth, a physical model can guide the choice of simplified mathematical and statistical models. Preliminary results have been recently communicated in [61], based on in situ measurements coupled with simulation tools (e.g., ray-tracing techniques). A second challenge is to develop unmixing models that take heterogeneity of the medium into account. Heterogeneous regions consist of combinations of linear, weakly non-linear and strongly non-linear pixels. The detection strategies detailed above might be one solution to tackle this problem since they are able to locate the areas where a non-linear model may outperform a linear model and vice-versa. Another approach adopted in [58], [59], which works well when there are only a few non-linear subregions, consists of using a statistical outlier approach to identify the non-linear pixels. Moreover, as any nonlinear blind source separation problem, deriving flexible unsupervised unmixing algorithms is still a major challenge, especially if one wants to go one step further than a crude pixel-by-pixel analysis by exploiting spatial information inherent to these images. Finally, we observe that the presence of nonlinearity in the observed spectra is closely related to the number R of endmembers which is usually unknown. For example, in analogy to kernelization in machine learning, after non-linear transformation, a nonlinear mixture of R components can often be represented as a linear mixture of $\tilde{R}$ endmembers, with $\tilde{R} > R$. Recent advances in manifold learning and dimensionality estimation are promising approaches to the non-linear unmixing problem.

References

[1] J. M. Bioucas-Dias, A. Plaza, N. Dobigeon, M. Parente, Q. Du, P. Gader, and J. Chanussot, "Hyperspectral unmixing overview: Geometrical, statistical, and sparse regression-based approaches," *IEEE J. Sel. Topics Appl. Earth Observations and Remote Sens.*, vol. 5, no. 2, pp. 354–379, April 2012.

[2] B. W. Hapke, "Bidirectional reflectance spectroscopy. I. Theory," *J. Geophys. Res.*, vol. 86, pp. 3039–3054, 1981.

[3] B. Hapke, *Theory of Reflectance and Emittance Spectroscopy*. Cambridge, UK: Cambridge Univ. Press, 1993.

[4] Y. Altmann, N. Dobigeon, S. McLaughlin, and J.-Y. Tourneret, "Nonlinear spectral unmixing of hyperspectral images using Gaussian processes," *IEEE Trans. Signal Process.*, vol. 61, no. 10, pp. 2442–2453, May 2013.

[5] T. Ray and B. Murray, "Nonlinear spectral mixing in desert vegetation," *Remote Sens. Environment*, vol. 55, pp. 59–64, 1996.

[6] J.-P. Combe, P. Launeau, V. Carrère, D. Despan, V. Mǐèder, L. Barillé, and C. Sotin, "Mapping microphytobenthos biomass by non-linear inversion of visible-infrared hyperspectral images," *Remote Sens. Environment*, vol. 98, no. 4, pp. 371–387, 2005.

[7] W. Liu and E. Y. Wu, "Comparison of non-linear mixture models: sub-pixel classification," *Remote Sens. Environment*, vol. 18, no. 2, pp. 145–154, Jan. 2005.

[8] K. Arai, "Nonlinear mixture model of mixed pixels in remote sensing satellite images based on Monte Carlo simulation," *Advances in Space Research*, vol. 41, no. 11, pp. 1715–1723, 2008.

[9] W. Fan, B. Hu, J. Miller, and M. Li, "Comparative study between a new nonlinear model and common linear model for analysing laboratory simulated-forest hyperspectral data," *Int. J. Remote Sens.*, vol. 30, no. 11, pp. 2951–2962, June 2009.

[10] B. Somers, K. Cools, S. Delalieux, J. Stuckens, D. V. der Zande, W. W. Verstraeten, and P. Coppin, "Nonlinear hyperspectral mixture analysis for tree cover estimates in orchards," *Remote Sens. Environment*, vol. 113, pp. 1183–1193, Feb. 2009.

[11] N. Keshava and J. F. Mustard, "Spectral unmixing," *IEEE Signal Process. Mag.*, vol. 19, no. 1, pp. 44–57, Jan. 2002.

[12] R. B. Singer and T. B. McCord, "Mars: Large scale mixing of bright and dark surface materials and implications for analysis of spectral reflectance," in *Proc. 10th Lunar and Planetary Sci. Conf.*, March 1979, pp. 1835–1848.

[13] R. N. Clark and T. L. Roush, "Reflectance spectroscopy: Quantitative analysis techniques for remote sensing applications," *J. Geophys. Res.*, vol. 89, no. 7, pp. 6329–6340, 1984.

[14] D. B. Nash and J. E. Conel, "Spectral reflectance systematics for mixtures of powdered hypersthene, labradorite, and ilmenite," *J. Geophys. Res.*, vol. 79, pp. 1615–1621, 1974.

[15] J. F. Mustard and C. M. Pieters, "Photometric phase functions of common geologic minerals and applications to quantitative analysis of mineral mixture reflectance spectra," *J. Geophys. Res.*, vol. 94, no. B10, pp. 13,619–13,634, Oct. 1989.

[16] B. T. Draine, "The discrete-dipole approximation and its application to interstellar graphite grains," *Astrophysical Journal*, vol. 333, pp. 848–872, Oct. 1988.

[17] Y. Shkuratov, L. Starukhina, H. Hoffmann, and G. Arnold, "A model of spectral albedo of particulate surfaces: implication to optical properties of the Moon," *Icarus*, vol. 137, no. 2, pp. 235–246, 1999.

[18] J. M. P. Nascimento and J. M. Bioucas-Dias, "Unmixing hyperspectral intimate mixtures," in *Proc. SPIE Image and Signal Processing for Remote Sensing XVI*, L. Bruzzone, Ed., vol. 74830. SPIE, Oct. 2010, p. 78300C.

[19] R. Close, P. Gader, A. Zare, J. Wilson, and D. Dranishnikov, "Endmember extraction using the physics-based multi-mixture pixel model," in *Proc. SPIE Imaging Spectrometry XVII*, S. S. Shen and P. E. Lewis, Eds., vol. 8515. San Diego, California, USA: SPIE, Aug. 2012, pp. 85 150L–14.

[20] J. M. P. Nascimento and J. M. Bioucas-Dias, "Nonlinear mixture model for hyperspectral unmixing," in *Proc. SPIE Image and Signal Processing for Remote Sensing XV*, L. Bruzzone, C. Notarnicola, and F. Posa, Eds., vol. 7477, no. 1. SPIE, 2009, p. 74770I.

[21] N. Raksuntorn and Q. Du, "Nonlinear spectral mixture analysis for hyperspectral imagery in an unknown environment," *IEEE Geosci. and Remote Sensing Lett.*, vol. 7, no. 4, pp. 836–840, 2010.

[22] A. Halimi, Y. Altmann, N. Dobigeon, and J.-Y. Tourneret, "Nonlinear unmixing of hyperspectral images using a generalized bilinear model," *IEEE Trans. Geosci. and Remote Sensing*, vol. 49, no. 11, pp. 4153–4162, Nov. 2011.

[23] W.-K. Ma, J. M. Bioucas-Dias, P. Gader, T.-H. Chan, N. Gillis, A. Plaza, A. Ambikapathi, and C.-Y. Chi, "Signal processing perspective on hyperspectral unmixing," *IEEE Signal Process. Mag.*, 2013, this issue.

[24] I. Meganem, P. Déliot, X. Briottet, Y. Deville, and S. Hosseini, "Linear-quadratic mixing model for reflectances in urban environments," *IEEE Trans. Geosci. and Remote Sensing*, 2013, to appear.

[25] R. Close, P. Gader, J. Wilson, and A. Zare, "Using physics-based macroscopic and microscopic mixture models for hyperspectral pixel unmixing," in *Proc. SPIE Algorithms and Technologies for Multispectral, Hyperspectral, and Ultraspectral Imagery XVIII*, S. S. Shen and P. E. Lewis, Eds., vol. 8390. Baltimore, Maryland, USA: SPIE, April 2012, pp. 83 901L–83 901L–13.

[26] Y. Altmann, A. Halimi, N. Dobigeon, and J.-Y. Tourneret, "Supervised nonlinear spectral unmixing using a post-nonlinear mixing model for hyperspectral imagery," *IEEE Trans. Image Process.*, vol. 21, no. 6, pp. 3017–3025, June 2012.

[27] D. Burazerovic, R. Heylen, B. Geens, S. Sterckx, and P. Scheunders, "Detecting the adjacency effect in hyperspectral imagery with spectral unmixing techniques," *IEEE J. Sel. Topics Appl. Earth Observations and Remote Sens.*, vol. 6, no. 3, pp. 1070–1078, June 2013.

[28] K. J. Guilfoyle, M. L. Althouse, and C.-I. Chang, "A quantitative and comparative analysis of linear and nonlinear spectral mixture models using radial basis function neural networks," *IEEE Trans. Geosci. and Remote Sensing*, vol. 39, no. 8, pp. 2314–2318, Aug. 2001.

[29] Y. Altmann, N. Dobigeon, S. McLaughlin, and J.-Y. Tourneret, "Nonlinear unmixing of hyperspectral images using radial basis functions and orthogonal least squares," in *Proc. IEEE Int. Conf. Geosci. Remote Sens. (IGARSS)*, Vancouver, Canada, July 2011, pp. 1151–1154.

[30] J. Plaza, P. Martinez, R. Perez, and A. Plaza, "Nonlinear neural network mixture models for fractional abundance estimation in AVIRIS hyperspectral images," in *Proc. XIII NASA/Jet Propulsion Laboratory Airborne Earth Science Workshop*, Pasadena, CA, USA, 2004.

[31] J. Plaza, A. Plaza, R. Perez, and P. Martinez, "Automated generation of semi-labeled training samples for nonlinear neural network-based abundance estimation in hyperspectral data," in *Proc. IEEE Int. Conf. Geosci. Remote Sens. (IGARSS)*, 2005, pp. 345–350.

[32] J. Plaza, A. Plaza, R. Pérez, and P. Martinez, "Joint linear/nonlinear spectral unmixing of hyperspectral image data," in *Proc. IEEE Int. Conf. Geosci. Remote Sens. (IGARSS)*, 2007, pp. 4037–4040.

[33] J. Plaza, A. Plaza, Rosa, Perez, and P. Martinez, "On the use of small training sets for neural network-based characterization of mixed pixels in remotely sensed hyperspectral images," *Pattern Recognition*, vol. 42, pp. 3032–3045, 2009.

[34] A. Halimi, Y. Altmann, N. Dobigeon, and J.-Y. Tourneret, "Unmixing hyperspectral images using the generalized bilinear model," in *Proc. IEEE Int. Conf. Geosci. Remote Sens. (IGARSS)*, Vancouver, Canada, July 2011, pp. 1886–1889.

[35] D. C. Heinz and C. -I Chang, "Fully constrained least-squares linear spectral mixture analysis method for material quantification in hyperspectral imagery," *IEEE Trans. Geosci. and Remote Sensing*, vol. 29, no. 3, pp. 529–545, March 2001.

[36] P. Gader, D. Dranishnikov, A. Zare, and J. Chanussot, "A sparsity promoting bilinear unmixing model," in *Proc. IEEE GRSS Workshop Hyperspectral Image SIgnal Process.: Evolution in Remote Sens. (WHISPERS)*, Shanghai, China, June 2012.

[37] A. Zare and P. Gader, "Sparsity promoting iterated constrained endmember detection in hyperspectral imagery," *IEEE Geosci. and Remote Sensing Lett.*, vol. 4, no. 3, pp. 446–450, July 2007.

[38] N. Yokoya, J. Chanussot, and A. Iwasaki, "Generalized bilinear model based nonlinear unmixing using semi-nonnegative matrix factorization," in *Proc. IEEE Int. Conf. Geosci. Remote Sens. (IGARSS)*, Munich, Germany, 2012, pp. 1365–1368.

[39] Y. Altmann, N. Dobigeon, and J.-Y. Tourneret, "Unsupervised post-nonlinear unmixing of hyperspectral images using a Hamiltonian Monte Carlo algorithm," *IEEE Trans. Image Process.*, 2013, submitted.

[40] R. Heylen and P. Scheunders, "Calculation of geodesic distances in nonlinear mixing models: Application to the generalized bilinear model," *IEEE Geosci. and Remote Sensing Lett.*, vol. 9, no. 4, pp. 644–648, July 2012.

[41] J. Plaza, A. Plaza, P. Martinez, and R. Perez, "Nonlinear mixture models for analyzing laboratory simulated-forest hyperspectral data," *Proc. SPIE Image and Signal Processing for Remote Sensing IX*, vol. 5238, pp. 480–487, 2004.

[42] P.-X. Li, B. Wu, and L. Zhang, "Abundance estimation from hyperspectral image based on probabilistic outputs of multi-class support vector machines," in *Proc. IEEE Int. Conf. Geosci. Remote Sens. (IGARSS)*, 2005, pp. 4315–4318.

[43] R. Heylen, D. Burazerovic, and P. Scheunders, "Non-linear spectral unmixing by geodesic simplex volume maximization," *IEEE J. Sel. Topics Signal Process.*, vol. 5, no. 3, pp. 534–542, June 2011.

[44] H. Nguyen, C. Richard, P. Honeine, and C. Theys, "Hyperspectral image unmixing using manifold learning methods. derivations and comparative tests," in *Proc. IEEE Int. Conf. Geosci. Remote Sens. (IGARSS)*, Munich, Germany, July 2012.

[45] G. Licciardi, X. Ceamanos, S. Doute, and J. Chanussot, "Unsupervised nonlinear spectral unmixing by means of NLPCA applied to hyperspectral imagery," in *Proc. IEEE Int. Conf. Geosci. Remote Sens. (IGARSS)*, Munich, Germany, July 2012, pp. 1369–1372.

[46] J. Broadwater, R. Chellappa, A. Banerjee, and P. Burlina, "Kernel fully constrained least squares abundance estimates," in *Proc. IEEE Int. Conf. Geosci. Remote Sens. (IGARSS)*, Barcelona, Spain, July 2007, pp. 4041–4044.

[47] J. Broadwater and A. Banerjee, "A comparison of kernel functions for intimate mixture models," in *Proc. IEEE GRSS Workshop Hyperspectral Image SIgnal Process.: Evolution in Remote Sens. (WHISPERS)*, Aug. 2009, pp. 1–4.

[48] J. Chen, C. Richard, and P. Honeine, "Nonlinear unmixing of hyperspectral data based on a linear-mixture/nonlinear-fluctuation model," *IEEE Trans. Signal Process.*, vol. 60, no. 2, pp. 480–492, Jan. 2013.

[49] ——, "Nonlinear abundance estimation of hyperspectral images with L1-norm spatial regularization," *IEEE Trans. Geosci. and Remote Sensing*, 2013, submitted.

[50] X. Li, J. Cui, and L. Zhao, "Blind nonlinear hyperspectral unmixing based on constrained kernel nonnegative matrix factorization," *Signal, Image and Video Processing*, pp. 1–13, 2012.

[51] N. H. Nguyen, J. Chen, C. Richard, P. Honeine, and C. Theys, "Supervised nonlinear unmixing of hyperspectral images using a pre-image methods," *EAS Publications Series*, vol. 59, pp. 417–437, 2013.

[52] P. Honeine and C. Richard, "Preimage problem in kernel-based machine learning," *IEEE Signal Processing Magazine*, vol. 28, no. 2, pp. 77–88, March 2011.

[53] RSI (Research Systems Inc.), *ENVI User's guide Version 4.0*, Boulder, CO 80301 USA, Sept. 2003.

[54] M. Winter, "Fast autonomous spectral end-member determination in hyperspectral data," in *Proc. 13th Int. Conf. on Applied Geologic Remote Sensing*, vol. 2, Vancouver, April 1999, pp. 337–344.

[55] Y. Altmann, N. Dobigeon, and J.-Y. Tourneret, "Nonlinearity detection in hyperspectral images using a polynomial post-nonlinear mixing model," *IEEE Trans. Image Process.*, vol. 22, no. 4, pp. 1267–1276, April 2013.

[56] N. Dobigeon, S. Moussaoui, M. Coulon, J.-Y. Tourneret, and A. O. Hero, "Joint Bayesian endmember extraction and linear unmixing for hyperspectral imagery," *IEEE Trans. Signal Process.*, vol. 57, no. 11, pp. 4355–4368, Nov. 2009.

[57] J. D. Gorman and A. O. Hero, "Lower bounds for parametric estimation with constraints," *IEEE Trans. Inf. Theory*, vol. 36, no. 6, pp. 1285 –1301, Nov. 1990.

[58] Y. Altmann, N. Dobigeon, S. McLaughlin, and J.-Y. Tourneret, "Residual component analysis of hyperspectral images - Application to joint nonlinear unmixing and nonlinearity detection," *IEEE Trans. Image Process.*, 2013, submitted.

[59] N. Dobigeon and C. Févotte, "Robust nonnegative matrix factorization for nonlinear unmixing of hyperspectral images," in *Proc. IEEE GRSS Workshop Hyperspectral Image SIgnal Process.: Evolution in Remote Sens. (WHISPERS)*, Gainesville, FL, June 2013.

[60] Y. Altmann, N. Dobigeon, J.-Y. Tourneret, and J. C. M. Bermudez, "A robust test for nonlinear mixture detection in hyperspectral images," in *Proc. IEEE Int. Conf. Acoust., Speech, and Signal Processing (ICASSP)*, Vancouver, Canada, June 2013, pp. 2149–2153.

[61] L. Tits, W. Delabastita, B. Somers, J. Farifteh, and P. Coppin, "First results of quantifying nonlinear mixing effects in heterogeneous forests: A modeling approach," in *Proc. IEEE Int. Conf. Geosci. Remote Sens. (IGARSS)*, 2012, pp. 7185–7188.